



Computational discovery of small drug-like compounds as potential inhibitors of SARS-CoV-2 main protease

Alexander M. Andrianov^a, Yuri V. Kornoushenko^a, Anna D. Karpenko^b, Ivan P. Bosko^b and Alexander V. Tuzikov^b

^aInstitute of Bioorganic Chemistry, National Academy of Sciences of Belarus, Minsk, Republic of Belarus; ^bUnited Institute of Informatics Problems, National Academy of Sciences of Belarus, Minsk, Republic of Belarus

Communicated by Ramaswamy H. Sarma

ABSTRACT

A computational approach to *in silico* drug discovery was carried out to identify small drug-like compounds able to show structural and functional mimicry of the high affinity ligand X77, potent non-covalent inhibitor of SARS-CoV-2 main protease (M^{Pro}). In doing so, the X77-mimetic candidates were predicted based on the crystal X77- M^{Pro} structure by a public web-oriented virtual screening platform Pharmit. Models of these candidates bound to SARS-CoV-2 M^{Pro} were generated by molecular docking, quantum chemical calculations and molecular dynamics simulations. At the final point, analysis of the interaction modes of the identified compounds with M^{Pro} and prediction of their binding affinity were carried out. Calculation revealed 5 top-ranking compounds that exhibited a high affinity to the active site of SARS-CoV-2 M^{Pro} . Insights into the ligand – M^{Pro} models indicate that all identified compounds may effectively block the binding pocket of SARS-CoV-2 M^{Pro} , in line with the low values of binding free energy and dissociation constant. Mechanism of binding of these compounds to M^{Pro} is mainly provided by van der Waals interactions with the functionally important residues of the enzyme, such as His-41, Met-49, Cys-145, Met-165, and Gln-189 that play a role of the binding hot spots assisting the predicted molecules to effectively interact with the M^{Pro} active site. The data obtained show that the identified X77-mimetic candidates may serve as good scaffolds for the design of novel antiviral agents able to target the active site of SARS-CoV-2 M^{Pro} .

ARTICLE HISTORY

Received 6 May 2020
Accepted 1 July 2020

KEYWORDS

Coronavirus SARS-CoV-2; COVID-19; main protease; SARS-CoV-2 inhibitors; virtual screening; molecular docking; quantum chemical calculations; antiviral drugs

Introduction

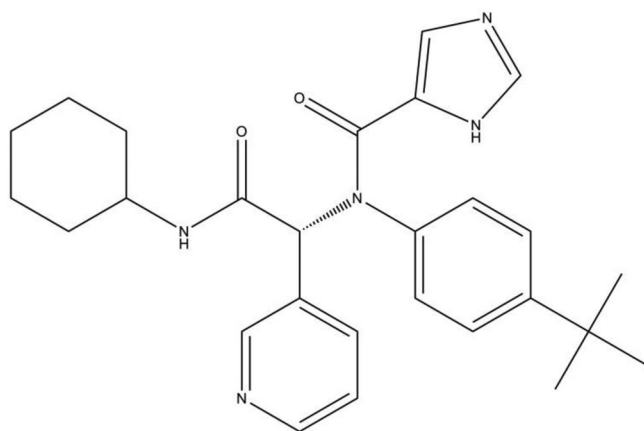
The recent outbreak of coronavirus infection in China caused by the SARS-CoV-2 virus associated with COVID-19 has become a matter of serious concern to the world community, as the number of infected people is constantly increasing with significant geographical spread. As of the beginning of June 2020, the World Health Organization reports over 6.9 million confirmed cases of infection and over 400 thousand deaths. Numerous attempts are being made to develop an effective antiviral vaccine and find new therapeutic agents against COVID-19. Studies of various aspects of SARS-CoV-2, including structure, mechanism of action, epidemiology and genome sequencing, have provided important information about the new virus (Boopathi et al., 2020; Chan et al., 2020; Lu et al., 2020). According to the data obtained (Chan et al., 2020; Lu et al., 2020), SARS-CoV-2 belongs to a large family of coronaviruses that infect humans and other animal species, causing many widespread and serious diseases, such as Severe Acute Respiratory Syndrome (SARS) and Middle East Respiratory Syndrome (MERS) (De Wit et al., 2016). The SARS-CoV-2 coronavirus genome is positive-sense, single-stranded RNA and consists of ~ 30,000 nucleotides, and its replicase gene encodes two overlapping polyproteins, pp1a and pp1ab, required for virus replication and transcription (Chen

et al., 2020). These polyproteins undergo extensive proteolytic processing by two cysteine proteases, namely papain-like protease PLpro and 3-chymotrypsin-like protease 3CLpro (also known as the main protease M^{Pro}) which is essential for mediating viral replication and transcription (Anand et al., 2002; Yang et al., 2003). The main protease digests polyprotein at no less than 11 conserved sites, starting with the autolytic cleavage of this enzyme itself from pp1a and pp1ab (Hegy & Ziebuhr, 2002). This indicates the extremely important role of M^{Pro} in the life virus cycle and makes this enzyme one of the most attractive targets for the development of effective antiviral drugs (Pillaiyar et al., 2016).

In the newest studies, SARS-CoV-2 M^{Pro} has been used as a target for screening clinically approved drugs as potential virus inhibitors in the hope of identifying drugs that are effective against COVID-19 (e.g. Adeoye et al., 2020; Babadaei et al., 2020; Enmozhi et al., 2020; Hendaus, 2020; Khan et al., 2020; Liu & Wang, 2020; Muralidharan et al., 2020; Rismanbaf, 2020; Yan et al., 2020; Zhijian et al., 2020; Zhou et al., 2020). Since the safety profiles of these drugs are well-documented, such an approach combining the structural design of drugs with virtual screening and molecular modeling methods can significantly facilitate and accelerate the detection of antiviral compounds with clinical potential in order to re-profile them for the

Table 1. Pharmacophore model of X77 used for virtual screening of the Pharmit chemical databases.

Pharmacophore type	Pharmacophore coordinates X, Y, Z (Å)			Pharmacophore radius (Å)
	X	Y	Z	
Aromatic group	-20.75	17.39	-28.53	R = 1.1
Aromatic group	-20.55	20.33	-31.86	R = 1.1
H-bond acceptor	-16.19	21.86	-26.88	R = 0.5
H-bond acceptor	-20.84	19.52	-32.66	R = 0.5
H-bond acceptor	-19.75	22.16	-29.14	R = 0.5
H-bond acceptor	-18.66	18.65	-25.94	R = 0.5
Hydrophobic group	-20.55	20.33	-31.86	R = 1.0



(R)-N-(4-tert-butylphenyl)-N-(2-(cyclohexylamino)-2-oxo-1-(pyridin-3-yl)ethyl)-1H-imidazole-5-carboxamide

Figure 1. Chemical structure of X77, potent non-covalent inhibitor of SARS-CoV-2 M^{Pro} (PDB ID: 6W63, <http://www.rcsb.org/pdb/>). The systematic name of this compound is given.

treatment of patients infected with a new type of coronavirus. However, taking into account SARS-CoV-2 mutations (Forster et al., 2020; Khailany et al., 2020; Pachetti et al., 2020; Yao et al., 2020), studies on the development of novel antiviral compounds capable of blocking the functionally important sites of the viral proteins are also extremely significant.

Determination of the high-resolution X-ray structures of SARS-CoV-2 main protease (M^{Pro}) in ligand-bound and unbound states (Berman et al., 2000; <http://www.rcsb.org/pdb/>) laid the foundation not only for understanding the function and molecular mechanism of the enzyme action, but also for developing novel effective SARS-CoV-2 inhibitors by direct methods of computer-aided drug design (e.g. Bhardwaj et al., 2020; Fischer et al., 2020; Gupta et al., 2020; Islam et al., 2020; Jin et al., 2020; Joshi et al., 2020; Khan et al., 2020; Olubiyi et al., 2020; Pant et al., 2020; Sarma et al., 2020; Ton et al., 2020; Vega-Valdez et al., 2020; Wahedi et al., 2020; Zhang et al., 2020). In particular, SARS-CoV-2 M^{Pro} structure in the complex with the high affinity ligand X77 that is potent non-covalent inhibitor of SARS-CoV-2 M^{Pro} was recently deposited in the Protein Data Bank (PDB ID: 6W63, <http://www.rcsb.org/pdb/>).

In this study, an integrated computational approach to *in silico* drug discovery was carried out to discover small drug-like compounds able to show structural and functional mimicry of the inhibitor X77. This computer-based approach included i) generation of pharmacophore model representing 3D-

arrangements of chemical functionalities that make X77 active towards the active site of SARS-CoV-2 M^{Pro}, (ii) shape/pharmacophore-based identification of the X77-mimetic candidates by a web-oriented virtual screening platform Pharmit (<http://pharmit.csb.pitt.edu>) allowing one to search for small molecules based on their structural and chemical similarity to another small molecule (Sunseri & Koes, 2016), (iii) identification of compounds satisfying the Lipinski's "rule of five" (Lipinski et al., 2001) that recognizes molecules with drug-like properties, (iv) molecular docking of these drug-like compounds with the enzyme active site, (v) prediction of the interaction modes dominating the binding; (vi) calculation of the values of binding free energy and dissociation constant (K_d) for the docking ligand – M^{Pro} models, (vii) optimization of these models using the semiempirical quantum chemical method PM7 (Stewart, 2013), (viii) molecular dynamics (MD) simulations of the identified compounds bound to M^{Pro}, (ix) calculation of the values of binding energy for the PM7-based and dynamic ligand – M^{Pro} models, and (x) selection of molecules most promising for biochemical assays.

As a result, an ensemble of hit compounds that bind to the active site of SARS-CoV-2 M^{Pro} and specifically interact with the functionally important residues of the enzyme was identified. These compounds are suggested to form good scaffolds for the development of novel, potent and broad drugs against COVID-19.

Methods and materials

Virtual screening

The Pharmit server software (Sunseri & Koes, 2016; <http://pharmit.csb.pitt.edu>) was used to generate the X77 pharmacophore model based on the X77 – M^{Pro} complex in crystal (PDB ID: 6w63; <https://www.rcsb.org>). This model (Table 1) was applied for virtual screening of small-molecule compounds able to block the X77-binding site of SARS-CoV-2 M^{Pro}. Virtual screening was performed in the 9 Pharmit molecular libraries containing over 213.5 million chemical structures (Sunseri & Koes, 2016; <http://pharmit.csb.pitt.edu>), resulting in a set of compounds that satisfied the X77 pharmacophore model (Table 1) and Lipinski's "rule of five" (Lipinski et al., 2001). These molecules were further screened by molecular docking and quantum chemical calculations to evaluate the affinity of their binding to SARS-CoV-2 M^{Pro} and identify molecules most promising for biochemical assays.

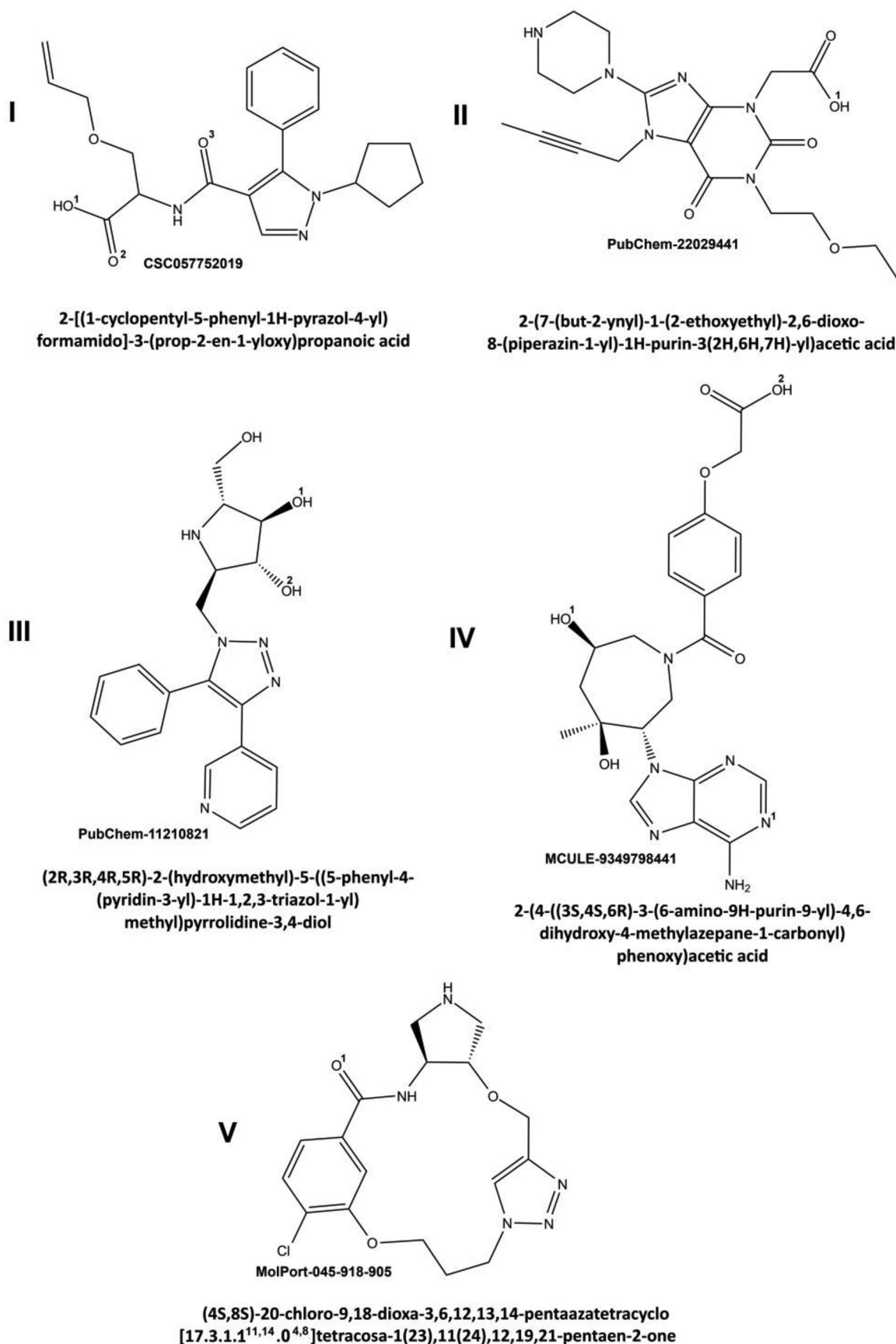


Figure 2. Chemical structures of the potential SARS-CoV-2 M^{Pro} inhibitors. The systematic names of the compounds, as well as the corresponding databases with codes for these molecules are given. The ligand functional groups participating in the formation of intermolecular hydrogen bonds are marked by superscript numbers (see the text and Table 4).

Table 2. Values of dissociation constant and binding energy calculated for the identified compounds and X77 bound to SARS-CoV-2 M^{Pro}.

Ligand	I	II	III	IV	V	X77
K_d^{-1} , (μ M)	0.006	0.039	0.157	2.0	2.65	0.057
$\Delta G_{\text{DOC}_3^2}$, (kcal/mol)	-11.65	-10.50	-9.64	-8.07	-7.90	-10.21
ΔH_{PM7^3} , (kcal/mol)	-80.1	-96.6	-90.7	-71.4	-53.78	-62.8
$\Delta G_{\text{MM/GBSA}^4}$, (kcal/mol)	-27.18 ± 6.53	-47.66 ± 4.33	-33.56 ± 5.88	-39.21 ± 3.83	-35.00 ± 3.71	-41.70 ± 4.28

Footnotes: ¹ The values of K_d calculated for the docking ligand – M^{Pro} models; ² The ΔG values estimated from those of K_d ; ³ The values of binding enthalpy calculated for the PM7-based complexes; ⁴ The values of binding energy calculated for the dynamic ligand – M^{Pro} models. The averages and standard deviations corresponding to these mean values are given.

Table 3. Physicochemical parameters of the X77-mimetic candidates associated with the Lipinski's "rule of five".

Ligand	Chemical formula	Molecular mass (Da)	LogP	Number of H-bond donors	Number of H-bond acceptors
I	C ₂₁ H ₂₅ N ₃ O ₄	384.00	2.225	3	6
II	C ₁₉ H ₂₆ N ₆ O ₅	419.00	-1.206	3	9
III	C ₁₉ H ₂₁ N ₅ O ₃	368.00	0.146	5	6
IV	C ₂₁ H ₂₄ N ₆ O ₆	456.00	0.071	5	11
V	C ₁₇ H ₂₀ ClN ₅ O ₃	378.00	-1.090	3	6

Molecular docking

Molecular docking of the predicted compounds with SARS-CoV-2 M^{Pro} was carried out by the QuickVina 2 program (Alhossary et al., 2015) in the approximation of rigid receptor and flexible ligands. The X77 inhibitor (Figure 1) was used in the calculations as a positive control. The 3D structure of this compound was isolated from the crystal X77 – M^{Pro} complex (the PDB ID: 6W63; <http://www.rcsb.org/pdb/>). The SARS-CoV-2 M^{Pro} and ligand structures were prepared by adding hydrogen atoms with the Open Babel software (http://openbabel.org/wiki/Main_Page) followed by their optimization in the UFF force field (Rappe et al., 1992). The ligands were docked to the crystal SARS-CoV-2 M^{Pro} structure using QuickVina 2 (Alhossary et al., 2015). The grid box included the X77-binding site of SARS-CoV-2 M^{Pro} and had the following parameters: $\Delta X = 19 \text{ \AA}$, $\Delta Y = 21 \text{ \AA}$, $\Delta Z = 23 \text{ \AA}$ centered at $X = -20 \text{ \AA}$, $Y = 19 \text{ \AA}$, $Z = -26 \text{ \AA}$; that is, the box volume was $19 \times 21 \times 23 = 9177 \text{ \AA}^3$. The value of "exhaustiveness" parameter defining number of individual sampling "runs" was set to 1000 (Alhossary et al., 2015).

Quantum chemical calculations

The quantum chemical optimization of the docked ligand – M^{Pro} structures was carried out using the semiempirical quantum chemical method PM7 (Stewart, 2013) associated with the MOPAC2016 software package (<http://OpenMOPAC.net>). Before the calculations, the ligand – M^{Pro} complexes were supplemented with hydrogen atoms and optimized in the UFF force field (Rappe et al., 1992). For this purpose, the Open Babel program (http://openbabel.org/wiki/Main_Page) was used. The calculations were performed in the COSMO solvation model (CONductor-like Screening MOdel) approximation (Klamt, 2005; Klamt et al., 2015; Klamt & Schüürmann, 1993) in an implicit solvent with water's dielectric constant of 78.4 (<http://OpenMOPAC.net>). To speed up the calculations, the Localized Molecular Orbitals method (Høyvik et al., 2012; Lehtola & Jónsson, 2013) available in MOPAC in the form of the linear scaling SCF MOZYME

algorithm (Stewart, 2013) was applied. The value of RMS gradient was set to 10 kcal/mol/Å.

Molecular dynamics simulations

The classical dynamics of the ligand – M^{Pro} complexes in water was made with the implementation of Amber18 using the Amber ff14SB force field (Case et al., 2020). The Antechamber module was employed to set the Gasteiger atomic partial charges (Case et al., 2020). To prepare the force field parameters, the general Amber GAFF force field (Wang et al., 2004) was used. Hydrogen atoms were added to M^{Pro} by the tleap program of the AmberTools18 package (Case et al., 2020). Initially, the ligand – M^{Pro} complexes were each placed in a cubical box with periodic boundary conditions. In addition to the ligand – M^{Pro} complex, the box for the MD simulations included TIP3P water (Jorgensen et al., 1983) as an explicit solvent, Na⁺ and Cl⁻ ions providing overall salt concentration of 0.10 M. After setting up the system, an energy minimization was performed using 500 steps of the steepest descent algorithm followed by 500 steps of the conjugate-gradient method. The backbone atoms of the complex assembly were then fixed by an additional harmonic potential with the force constant of 2.0 kcal/mol and the system was subject to the equilibration phase. The system equilibration was carried out in three consecutive stages: 1) the system was gradually heated from 0 K to 310 K for 1 ns in NVT ensemble using a Langevin thermostat with a collision frequency of 2.0 ps⁻¹ (Case et al., 2020); 2) pressure equilibration was made for 1 ns at 1.0 bar in NPT ensemble using Berendsen barostat with a 2.0 ps characteristic time (Case et al., 2020); 3) the constraints on the complex assembly were removed and the system was equilibrated again at 310 K over 0.5 ns under constant volume conditions. After equilibration was achieved, the MD simulations were carried out for 50 ns in NPT ensemble at temperature $T = 310 \text{ K}$ and $p = 1 \text{ bar}$. Bonds involving hydrogen atoms were constrained using SHAKE algorithm (Ryckaert et al., 1977) to achieve the integration time-step of 2 ps. Long-range electrostatic interactions were calculated using Particle Mesh Ewald (PME)

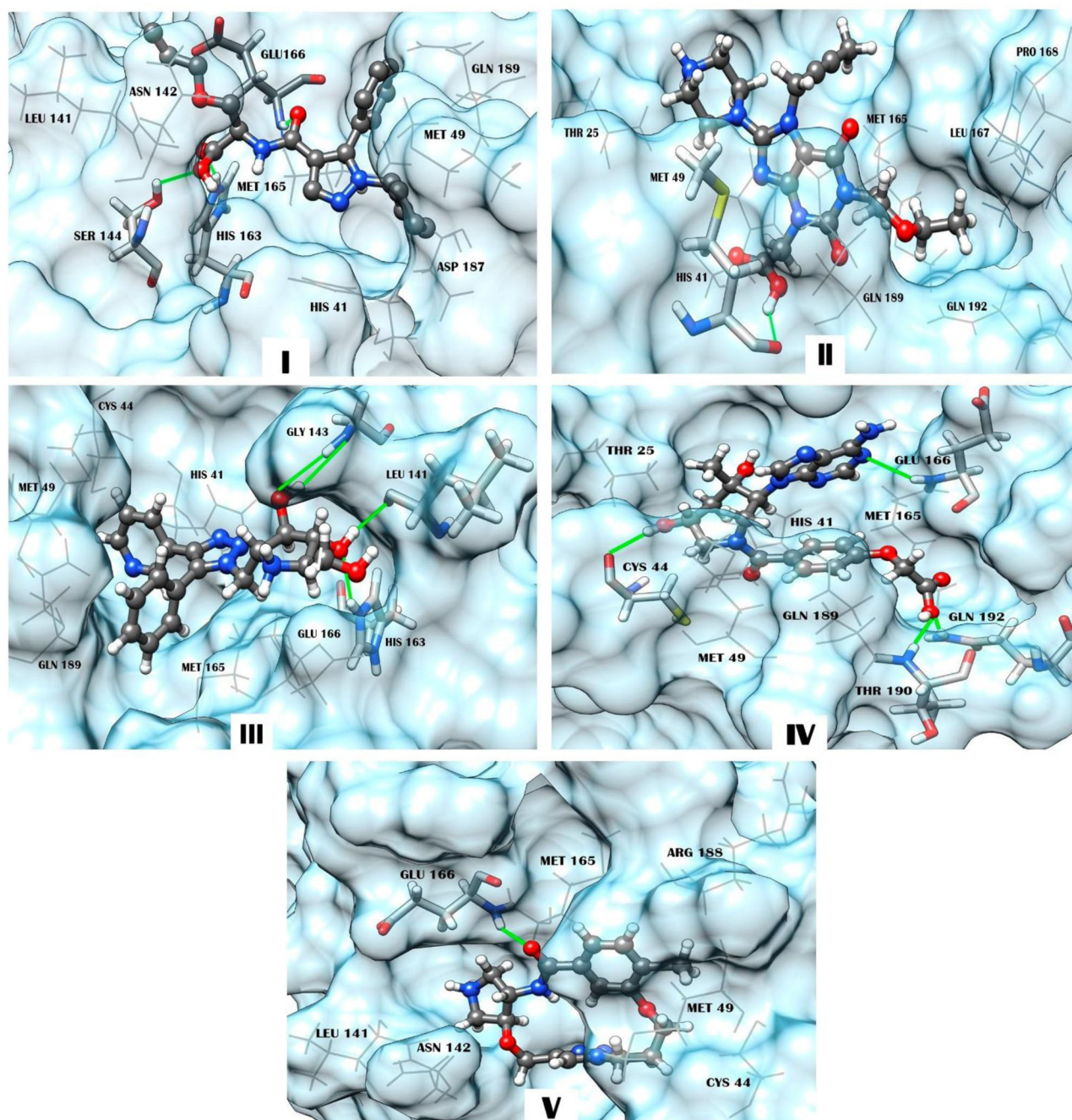


Figure 3. Structural complexes of compounds I, II, III, IV, and V with SARS-CoV-2 M^{Pro} generated by molecular docking. The compounds are represented by a ball-stick-ball model. The enzyme residues forming interatomic contacts with the ligands are indicated (Table 4). Residues of M^{Pro} involved in hydrogen bonding are noted using a stick model. Hydrogen bonds are shown by solid lines. A wire model is used to designate residues forming van der Waals contacts, salt bridges, and π - or T-stacking.

algorithm (Essmann et al., 1995). Coulomb interactions and van der Waals interactions were truncated at 8 Å.

Analysis of interaction modes and binding affinity profile

The binding modes of the predicted compounds to SARS-CoV-2 M^{Pro}, namely hydrogen bonds, salt bridges, van der Waals contacts, and π - π interactions were identified by the BINANA program (Durrant & McCammon, 2011). The ligand

poses in the docking ligand – M^{Pro} models were visualized with the program UCSF Chimera (Pettersen et al., 2004). To visualize van der Waals contacts, the program LigPlot (McDonald & Thornton, 1994) was employed. The values of K_d for the ligand – M^{Pro} structures were calculated using a neural-network-based scoring function NNScore 2.0 (Durrant & McCammon, 2011). The values of binding free energy were estimated from those of K_d by the formula $\Delta G = R \times T \times \ln(K_d)$ (where ΔG is the binding free energy, R is the universal gas constant, T is the absolute temperature equal to 310 K) (Sharma & First, 2009).

Table 4. Intermolecular interactions appearing in the structural complexes of the identified compounds with SARS-CoV-2 M^{Pro}.

Ligand	Hydrogen bond ¹	Van der Waals contacts ²	Salt bridges and π - π interactions ³
I	O ¹ ... **HN[S144] O ² ... **HN[H163] O ³ ... *HN[E166]	H41(3), M49(1), L141(3), N142(1), M165(6), E166(3), D187(2), Q189(1)	COO ... H163 H41 (T-stacking)
II	O ¹ H ... *O[M49]	T25(1), H41(2), M165(3), L167(1), P168(1), Q189(1), Q192(1)	—
III	O ¹ H ... *N[L141] O ² H ... *N[G143] O ² ... *NH[G143] O ¹ ... **HN[H163]	H41(4), C44(1), M49(1), M165(4), L141(2), N142(1), E166(2), Q189(5)	NCHC ... E166 H41 (T- и π -stacking)
IV	O ¹ H ... *O[C44] N ¹ ... *HN[E166] O ² ... *HN[T190] O ² ... **HN[Q192]	T25(2), H41(1), C44(1), M49(1), M165(3), Q189(4)	H41 (T-stacking)
V	O ¹ ... *HN[E166]	C44(2), M49(1), L141(1), N142(1), M165(4), E166(1), R188(1)	—

Footnotes: ¹Atoms of the ligands are shown first, followed by the corresponding atoms of SARS-CoV-2 M^{Pro} (M^{Pro} residues are in brackets in one-letter code). Symbol * denotes the atoms of the residue main chain, and symbol ** marks the atoms of the residue side chain. ²Amino acids of SARS-CoV-2 M^{Pro} forming van der Waals contacts with the ligands. The number of contacts is given in brackets. ³For salt bridges, the functional groups of ligands are shown first, followed by the residues of SARS-CoV-2 M^{Pro}. For π - or T-stacking, residue of SARS-CoV-2 M^{Pro} involved in these interactions is shown.

For the PM7-based complexes, the ligand-binding affinity was estimated in terms of the values of binding enthalpy ΔH calculated as the differences between the heats of formation of the ligand – M^{Pro} complexes and heats of formation of the ligand and M^{Pro} in the unbound states (Stewart, 2013; <http://OpenMOPAC.net>). Quantum chemical calculations of the ligand and M^{Pro} structures in the unbound states were performed using the computational protocol described above for the docking ligand – M^{Pro} models.

In the case of dynamic ligand – M^{Pro} models, the values of binding energy were calculated with Amber18 (Case et al., 2020) using the MM/GBSA method (Genheden & Ryde, 2015; Sun et al., 2014; Xu et al., 2013). The calculations were made for 200 snapshots extracted from the final 40 ns of the MD trajectories, by keeping the snapshots every 0.2 ns. The polar solvation energies were computed in continuum solvent using Poisson-Boltzmann continuum-solvation model with ionic strength of 0.10. The non-polar terms were estimated using solvent accessible surface areas (Case et al., 2020). Analysis of the MD trajectories was performed by the CPPTRAJ module of AmberTools 18 (Case et al., 2020).

Results and discussion

Shape/Pharmacophore-based virtual screening of the Pharmit databases resulted in 24 molecules that exhibited favorable binding energies (< -6 kcal/mol) and the values of root-mean-square deviations between the query features and the hit compound features less than 2 Å (Sunseri & Koes, 2016). Molecular docking of these molecules with the active site of M^{Pro} followed by quantum chemical calculations and MD simulations identified 5 top-ranking compounds (Figure 2) that showed a high-affinity binding in terms of K_d , binding free energy, and binding enthalpy (Table 2). This allowed one to consider these compounds as the most probable X77-mimetic candidates. Inspection of the physicochemical parameters of the predicted compounds (Table 3) providing such important characteristics for a potential drug as absorption, distribution, metabolism and excretion indicates that these molecules fully satisfy the requirements of the Lipinski's "rule of five" (Lipinski et al., 2001).

Insights into the docking ligand – M^{Pro} models (Figure 3) show that all identified X77-mimetic candidates form a wide network of intermolecular interactions involving amino acid residues of the binding pocket of M^{Pro}. In particular, compound I exhibiting the lower values of K_d and binding free

energy compared to the other predicted molecules and X77 (Table 2) forms 3 hydrogen bonds with the M^{Pro} residues Ser-144, His-163 and Glu-166, a salt bridge with His-163, and 20 van der Waals contacts with the active site residues His-41, Met-49, Leu-141, Asn-142, Met-165, Glu-166, Asp-187, and Gln-189 (Table 4). In addition to these direct interatomic contacts, compound I is also involved in specific π - π interaction with His-41 which is a part of the catalytic dyad of M^{Pro} formed by this residue and Cys-145 (Chang, 2010; Qamar et al., 2020). Examination of the intermolecular interaction profile calculated for the other identified compounds indicates (Table 4) that these molecules exhibit the modes of binding to SARS-CoV-2 M^{Pro} similar to those predicted for compound I. According to the data obtained, these binding modes are provided by hydrogen bonds, van der Waals contacts, salt bridges (compounds I and III) and π - π interactions between π -conjugated systems of the ligands and the side chain of His-41 (compounds I, III and IV) (Table 4, Figure 4). Among these binding modes, intermolecular van der Waals interactions are the major contributors to the ligand – M^{Pro} interface including significant residues of the enzyme active pocket (Table 4, Figure 4).

The efficiency of the intermolecular interactions of the X77-mimetic candidates with SARS-CoV-2 M^{Pro} is supported by the low values of K_d (0.006 μ M – 2.56 μ M) and binding free energies ($\Delta G \leq -7.9$ kcal/mol), indicating their high affinity with the catalytic site of the enzyme (Table 2). Analysis of the values of K_d and binding free energy calculated for the identified compounds shows that, given the calculation errors, they are comparable with those obtained for X77 using the identical computational protocol (Table 2).

So, the data of molecular docking show that all identified compounds (Figure 2) may effectively block the key residues of the M^{Pro} catalytic site, which is confirmed by the low values of binding free energy and K_d calculated for the docking ligand – M^{Pro} models (Table 2). This is also supported by the data of quantum chemical calculations which show that, excluding compound V, the values of binding enthalpy of the analyzed molecules to M^{Pro} are lower than that predicted for the control inhibitor X77 by the same computational parameters (Table 2).

In general, the data of MD simulations are in agreement with the principal conclusions made from the analysis of the static ligand – M^{Pro} complexes. These complexes are relatively stable within the MD simulations, as evidenced by the averages of binding energies and corresponding standard

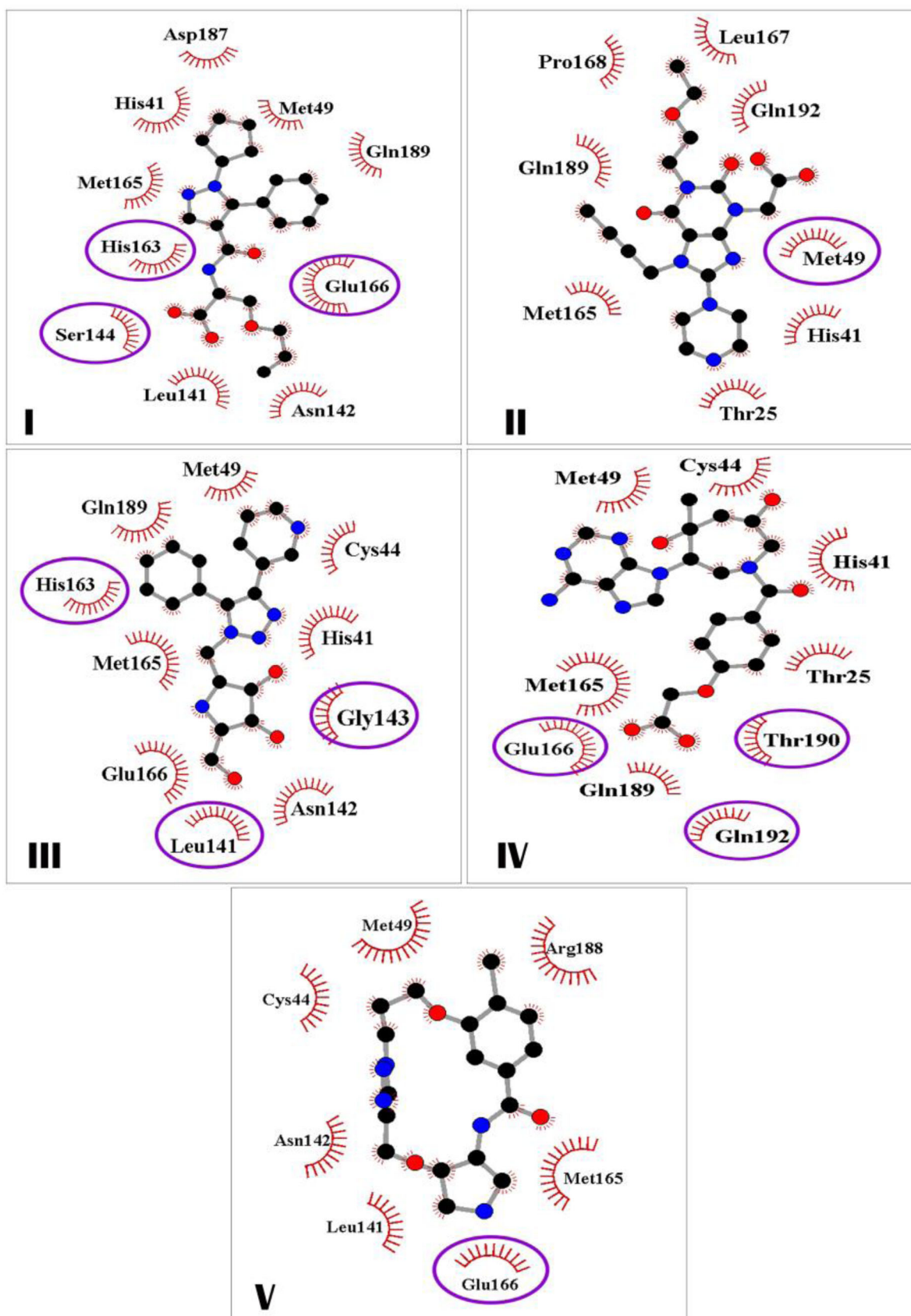


Figure 4. The SARS-CoV-2 M^{Pro} residues making direct interatomic contacts with compounds I, II, III, IV, and V. Residues involved in hydrogen bonding are marked by ellipses and highlighted in darker color.

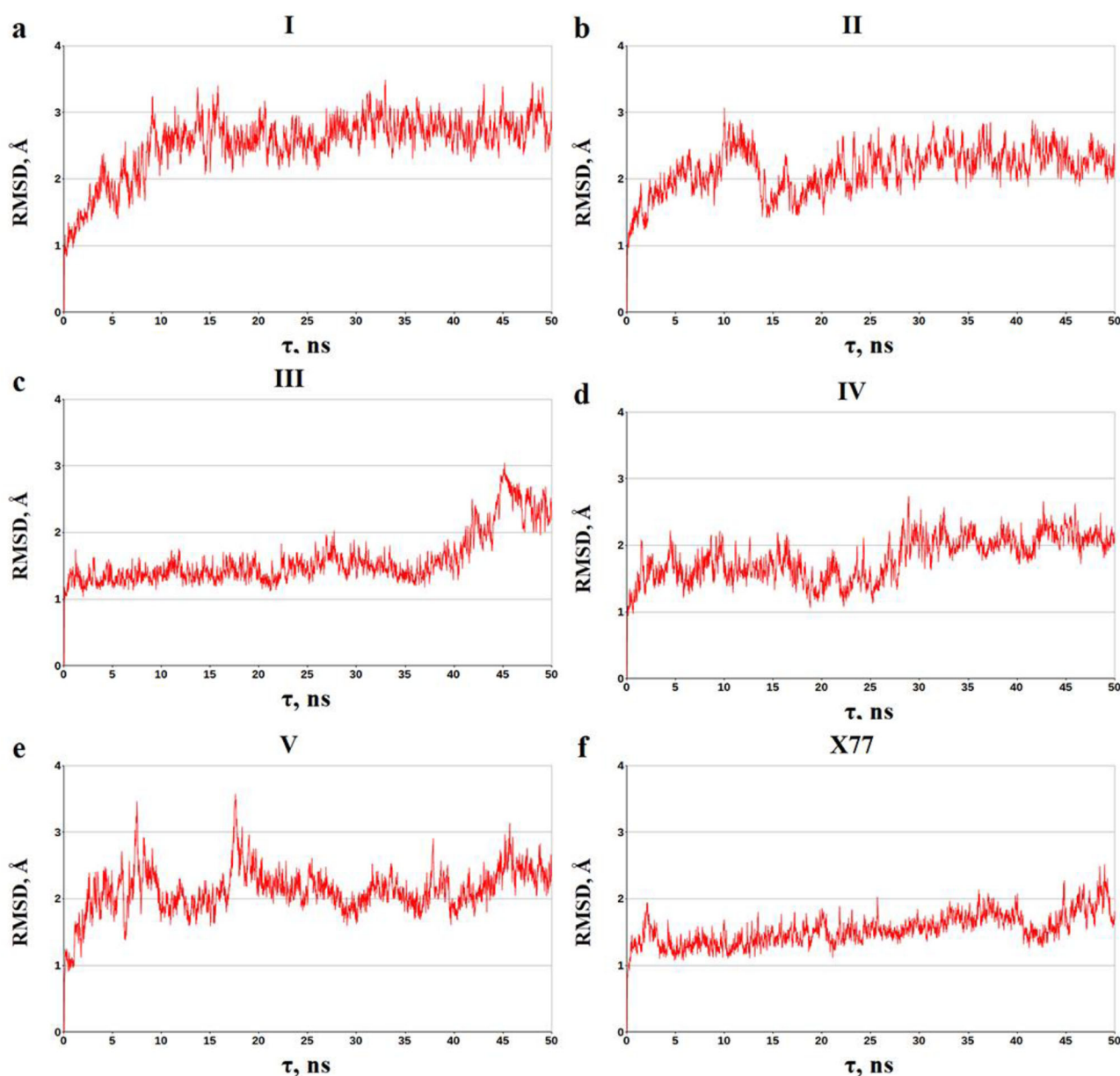


Figure 5. The time dependence of the RMSD (Å) calculated between all of the MD structures and the static models of the ligand – M^{Pro} complexes. The backbone atoms of M^{Pro} were used in the calculations.

deviations (Table 2). Given the MM/GBSA method errors (Genheden & Ryde, 2015; Sun et al., 2014; Xu et al., 2013), one can suggest that the dynamic ligand – M^{Pro} structures exhibit the averages of binding energy comparable with the value calculated for X77 by the identical computational protocol (Table 2). In favor of the relative stability of the dynamic ligand – M^{Pro} structures is also evidence of the data on the time dependence of the root-mean square deviations (RMSD) of the atomic positions for the dynamic and static models of the predicted compounds bound to M^{Pro} (Figure 5). Analysis of Figure 5 indicates that these complexes do not undergo significant structural rearrangements on the MD trajectories, which is confirmed by the averages of the RMSD calculated for the dynamic models of the identified molecules in the complexes with M^{Pro}. The mean values of RMSD and standard deviations, which are 2.54 ± 0.45 Å (compound

I), 2.15 ± 0.33 Å (compound II), 1.59 ± 0.39 Å (compound III), 1.81 ± 0.32 Å (compound IV), and 2.13 ± 0.34 Å (compound V), are close to those of 1.54 ± 0.23 Å obtained for the SARS-CoV-2 inhibitor X77 (Figure 5).

Examination of the data on the contributions of individual M^{Pro} amino-acid residues into the binding energy reveals the residues dominating the ligand – M^{Pro} interaction profile. Table 5 shows that these residues are His-41, Met-49 (excluding compound I), Cys-145, Met-165, and Gln-189. Importantly, it is those residues that are the major contributors to the X77 – M^{Pro} interaction (Table 5). Among these residues, it should first be noted the highly important His-41 and Cys-145 forming the catalytic dyad of SARS-CoV-2 M^{Pro} (Chang, 2010; Qamar et al., 2020). These data indicate that, despite the unbound SARS-CoV-2 M^{Pro} shows the higher mobility than a highly similar SARS-CoV M^{Pro} (Bzówka et al.,

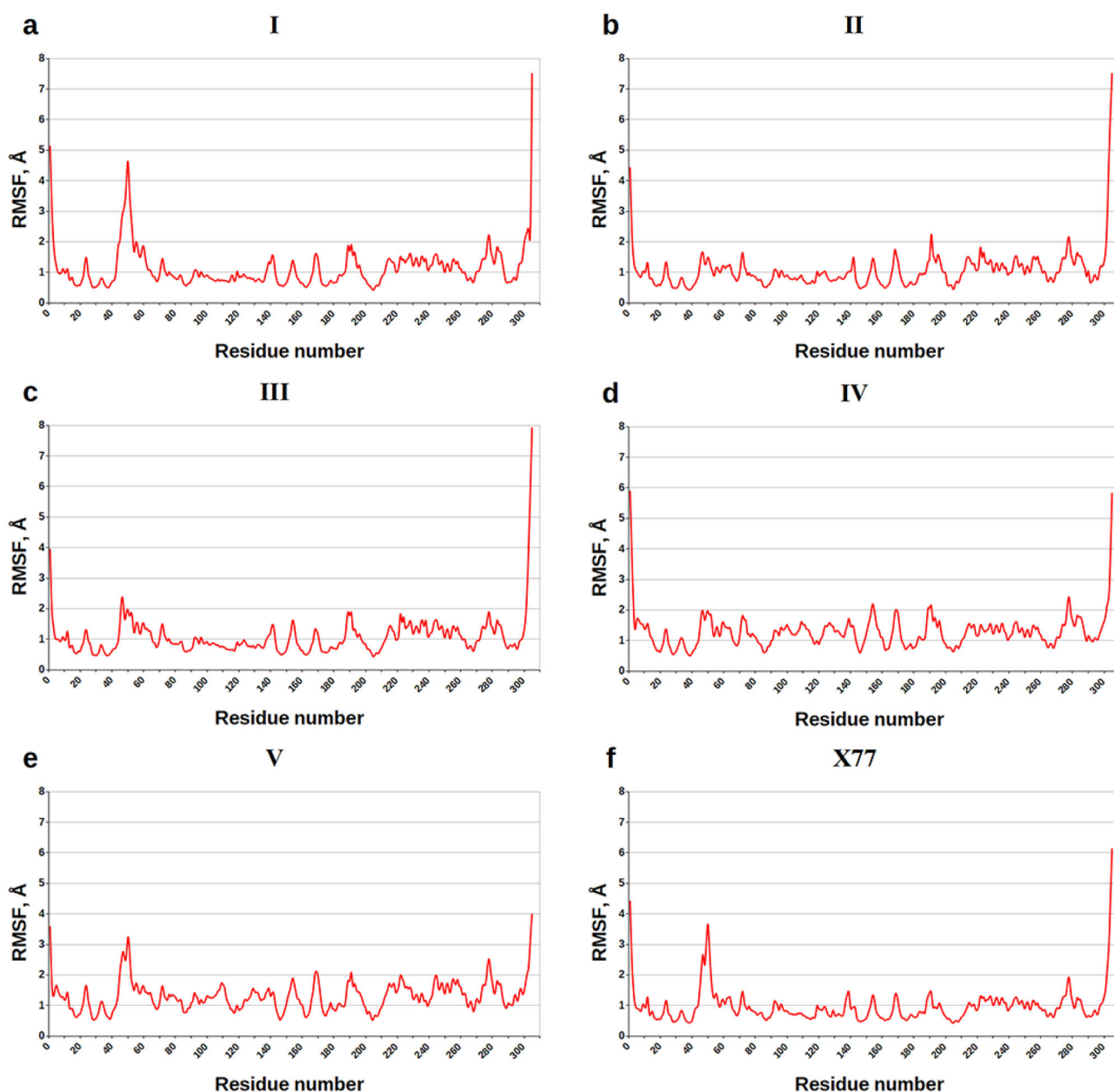


Figure 6. Values of RMSF (Å) for each residue along the amino-acid sequence of SARS-CoV-2 M^{Pro}.

2020), there are a number of the key anchoring residues assisting the identified compounds and X77 to effectively interact with the active site of the enzyme.

Figure 6 casts shed on the values of root-mean-square fluctuations (RMSF) of the individual residues of M^{Pro} indicating the flexibility of each amino acid during the MD simulations. Analysis of Figure 6 reveals that the majority of the M^{Pro} residues are positionally restrained on the MD trajectories, including the key anchoring residues His-41, Cys-145, Met-165, and Gln-189. The values of RMSF given for these binding hot spots in Table 6 testify to the quite small internal motions of these residues, in line with the data on their contributions into the binding energy (Table 5). The exception is Met-49 exhibiting the higher atomic fluctuations in the complexes with compound V and X77 compared with the other residues of the binding pocket of M^{Pro} (Figure 6, Table 6).

So, the findings of molecular docking, quantum chemical calculations and MD simulations suggest that the analyzed anti-SARS-CoV-2 (COVID-19) drug candidates expose the interaction modes and binding affinity profiles similar to those calculated for X77, potent, broad-spectrum inhibitor of coronavirus main protease including SARS-CoV-2 (PDB ID: 6W63, <http://www.rcsb.org/pdb/>).

Certainly, when analyzing the obtained data, it is necessary to keep in mind that all computational approaches for modeling ligand–protein complexes and estimating the binding affinity involve various approximations. They vary from simplified forms of the first-principles equations that are easier or faster to solve, to approximations limiting the size of the system, to fundamental approximations to the underlying equations that are required to achieve any solution to them at all. Nevertheless, the findings of comparative analysis of the X77 – M^{Pro} complexes constructed by the X-

Table 5. Averages of the binding energy for the amino-acid residues of M^{Pro} bound to the identified compounds and X77.

Residue of M ^{Pro}	I	II	III	IV	V	X77
Residue Contribution to the Binding Energy (kcal/mol) ^{1, 2, 3}						
Thr-25	–	–0.40 ± 0.18	–0.52 ± 0.45	–0.81 ± 0.28	–0.47 ± 0.32	–
Leu-27	–	–0.73 ± 0.20	–0.62 ± 0.46	–1.04 ± 0.36	–0.96 ± 0.29	–0.67 ± 0.28
His-41	–0.50 ± 0.38	–1.55 ± 0.39	–1.50 ± 0.61	–2.17 ± 0.68	–2.77 ± 0.66	–1.40 ± 0.36
Val-42	–	–	–	–	–0.47 ± 0.27	–
Cys-44	–	–	–0.59 ± 0.53	–0.59 ± 0.33	–0.78 ± 0.35	–
Thr-45	–	–	–0.41 ± 0.38	–	–	–
Ser-46	–	–	–0.58 ± 0.50	–0.75 ± 0.61	–	–
Met-49	–	–2.09 ± 0.68	–1.99 ± 0.65	–2.24 ± 0.48	–1.41 ± 0.63	–0.96 ± 0.64
Pro-52	–	–	–	–	–0.52 ± 0.28	–
Leu-141	–	–	–	–	–	–0.52 ± 0.27
Asn-142	–	–	–	–	–	–0.55 ± 0.36
Ser-144	–	–	–	–	–	–0.41 ± 0.17
Cys-145	–0.48 ± 0.34	–1.29 ± 0.31	–0.55 ± 0.39	–0.77 ± 0.30	–0.74 ± 0.28	–1.21 ± 0.34
Met-165	–1.73 ± 0.72	–2.64 ± 0.53	–1.01 ± 0.64	–1.24 ± 0.44	–0.87 ± 0.32	–1.97 ± 0.42
Glu-166	–	–0.57 ± 0.37	–	–	–	–0.59 ± 0.56
Leu-167	–	–0.65 ± 0.34	–	–	–	–
Pro-168	–0.67 ± 0.77	–0.70 ± 0.35	–	–	–	–0.87 ± 0.40
Asp-187	–0.40 ± 0.38	–0.69 ± 0.32	–0.60 ± 0.49	–0.57 ± 0.46	–0.42 ± 0.43	–
Arg-188	–	–0.60 ± 0.36	–	–	–	–
Gln-189	–1.25 ± 0.72	–1.24 ± 0.55	–0.74 ± 0.64	–0.82 ± 0.50	–0.73 ± 0.57	–0.71 ± 0.43
Ala-191	–	–0.44 ± 0.29	–	–	–	–
Ligand ⁴	–19.94 ± 4.08	–31.66 ± 2.60	–22.83 ± 3.65	–26.25 ± 2.26	–23.56 ± 2.14	–29.39 ± 2.50

Footnotes: ¹ Data for the SARS-CoV-2 M^{Pro} residues with the binding energy ≤ -0.4 kcal/mol are presented. ² The averages of the residue contributions to the binding energy and corresponding standard deviations are given. ³ The M^{Pro} residues dominating the ligand – M^{Pro} interaction are highlighted by bold. ⁴ The ligand contributions to the binding energy are presented.

ray crystallography and molecular docking (Figure 7) indicate simulations (Table 2). From the data of Table 2, the analyzed

Table 6. Values of RMSF for the M^{Pro} residues contributing to the binding energy.

Residue of M ^{Pro}	Compound						X77
	I	II	III	IV	V		
Values of RMSF (Å) for the individual residues of M ^{Pro}							
Thr-25	–	0.90	0.98	0.96	1.20	–	
Leu-27	–	0.60	0.66	0.64	0.70	0.58	
His-41	0.72	0.58	0.69	0.68	0.85	0.69	
Val-42	–	–	–	–	0.94	–	
Cys-44	–	–	0.96	0.98	1.42	–	
Thr-45	–	–	1.51	–	–	–	
Ser-46	–	–	2.26	1.87	–	–	
Met-49	–	1.30	1.83	1.84	2.58	2.97	
Pro-52	–	–	–	–	2.00	–	
Leu-141	–	–	–	–	–	0.92	
Asn-142	–	–	–	–	–	0.95	
Ser-144	–	–	–	–	–	0.61	
Cys-145	0.62	0.55	0.58	0.72	0.66	0.50	
Met-165	0.70	0.72	0.64	0.91	0.90	0.60	
Glu-166	–	0.99	–	–	–	0.72	
Leu-167	–	1.29	–	–	–	–	
Pro-168	1.52	1.74	–	–	–	1.30	
Asp-187	1.00	0.95	1.06	1.09	1.02	–	
Arg-188	–	1.11	–	–	–	–	
Gln-189	1.88	1.35	1.89	2.05	1.82	1.30	
Ala-191	–	2.25	–	–	–	–	

good prediction accuracy of the computational algorithm used in the calculations, suggesting that the data obtained for the identified compounds by molecular docking, quantum chemical calculations and MD simulations adequately describe the principal geometric and energy characteristics of their complexes with SARS-CoV-2 M^{Pro}.

Thus, the data on the intermolecular interaction network (Tables 4 and 5) are in line with the results of binding affinity prediction obtained for the ligand – M^{Pro} complexes using molecular docking, quantum chemical calculations and MD

complexes show the low values of K_d and binding energies, suggesting strong attachment of the identified X77-mimetic candidates to SARS-CoV-2 M^{Pro}. These small drug-like molecules are therefore promising candidates for further detailed experimental evaluation. However, it is clear that, despite promising *in silico* profile, the analyzed compounds are only starting points for the development of new highly potent drug candidates. In this connection, before biochemical assays, these compounds should go through a lead optimization, iterative process of altering the molecule structure to

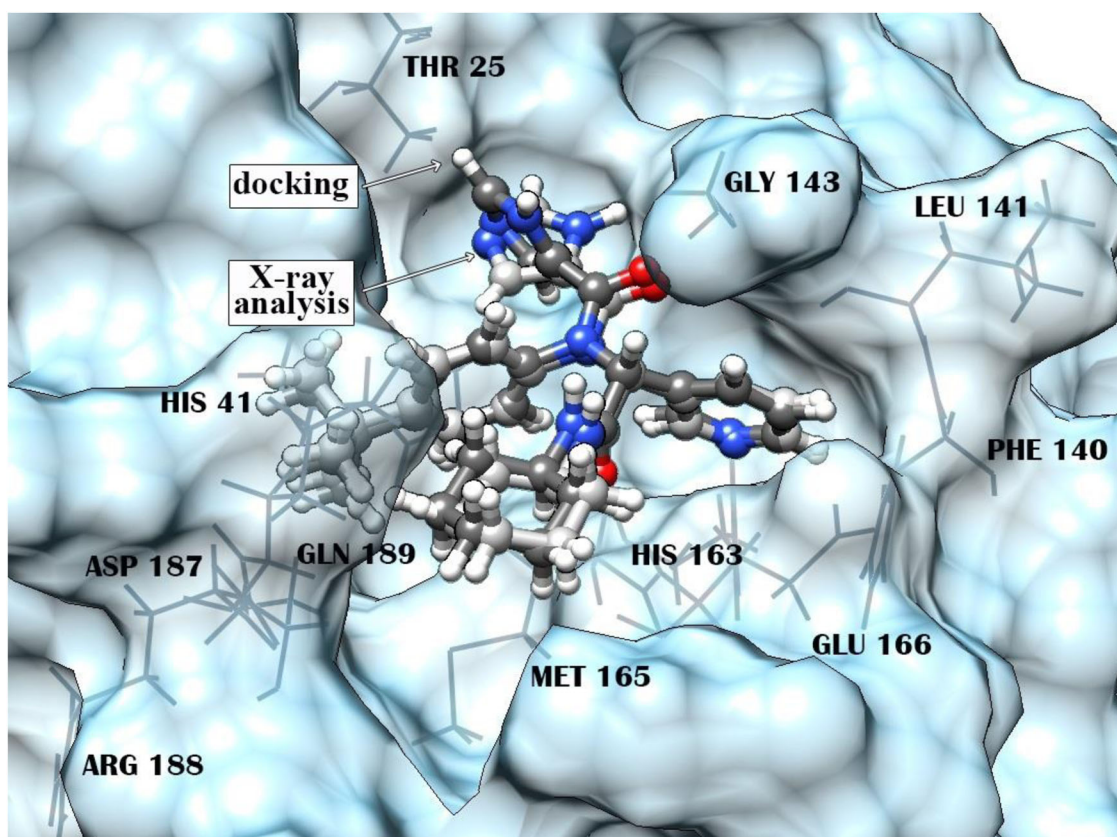


Figure 7. Superposition of the X77 – M^{Pro} complexes constructed using X-ray crystallography and molecular docking. The root-mean-square deviation between the atomic coordinates of the X77 inhibitor in the calculated and experimental structures is 0.63 Å. Residues of M^{Pro} forming direct interatomic contacts with X77 are marked by a wire model.

identify their chemical modifications with improved antiviral potency and ADMET parameters. For this purpose, the modern QSAR methods commonly used as a lead optimization approach in drug discovery may be applied (Golbraikh et al., 2017; Kuseva et al., 2019; Schultz et al., 2018).

Conclusions

Shape/Pharmacophore-based virtual screening combined with molecular docking, quantum chemical calculation and MD simulations revealed 5 top-ranking compounds that exhibited a high affinity to the catalytic site of SARS-CoV-2 M^{Pro}, allowing one to consider these small drug-like molecules as the most promising X77-mimetic candidates. Insights into the ligand – M^{Pro} models indicate that all identified compounds may specifically and effectively block the active site of SARS-CoV-2 M^{Pro}, in line with the low values of dissociation constants and binding energies. Mechanism of binding of these compounds to M^{Pro} is mainly provided by van der Waals interactions with the functionally important residues of the enzyme, such as His-41, Met-49, Cys-145, Met-165, and Gln-189 that play a role of the binding hot spots assisting the predicted molecules to effectively interact with the M^{Pro} active site.

Taken together, the data obtained show that the identified X77-mimetic candidates may serve as good scaffolds for

the design of novel antiviral agents able to target the active pocket of SARS-CoV-2 M^{Pro}.

Disclosure statement

No potential conflict of interest was reported by the author(s).

Funding

This study was funded by grants from the State Program of Scientific Research “Convergence 2020” (subprogram “Consolidation”, project 3.08) and the Belarusian Republican Foundation for Fundamental Research (project X20MC-006).

References

- Adeoye, A. O., Oso, B. J., Olaoye, I. F., Tijjani, H., & Adebayo, A. I. (2020). Repurposing of chloroquine and some clinically approved antiviral drugs as effective therapeutics to prevent cellular entry and replication of coronavirus. *Journal of Biomolecular Structure & Dynamics*. <https://doi.org/10.1080/07391102.2020.1765876>
- Alhossary, A., Handoko, S. D., Mu, Y., & Kwok, C. K. (2015). Fast, accurate, and reliable molecular docking with QuickVina 2. *Bioinformatics (Oxford, England)*, 31(13), 2214–2216. <https://doi.org/10.1093/bioinformatics/btv082>
- Anand, K., Palm, G. J., Mesters, J. R., Siddell, S. G., Ziebuhr, J., & Hilgenfeld, R. (2002). Structure of coronavirus main proteinase reveals combination of a chymotrypsin fold with an extra alpha-helical

- domain. *The EMBO Journal*, 21(13), 3213–3224. <https://doi.org/10.1093/emboj/cdf327>
- Babadai, M. M. N., Hasan, A., Vahdani, Y., Bloukh, S. H., Sharifi, M., Kachooei, E., Haghghat, S., & Falahati, M. (2020). Development of remdesivir repositioning as a nucleotide analog against COVID-19 RNA dependent RNA polymerase. *Journal of Biomolecular Structure & Dynamics*. <https://doi.org/10.1080/07391102.2020.1767210>
- Berman, H. M., Westbrook, J., Feng, Z., Gilliland, G., Bhat, T. N., Weissig, H., Shindyalov, I. N., & Bourne, P. E. (2000). The protein data bank. *Nucleic Acids Research*, 28(1), 235–242. <https://doi.org/10.1093/nar/28.1.235>
- Bhardwaj, V. K., Singh, R., Sharma, J., Rajendran, V., Purohit, R., & Kumar, S. (2020). Identification of bioactive molecules from Tea plant as SARS-CoV-2 main protease inhibitors. *Journal of Biomolecular Structure & Dynamics*. <https://doi.org/10.1080/07391102.2020.1766572>
- Boopathi, S., Poma, A. B., & Kolandaivel, P. (2020). Novel 2019 coronavirus structure, mechanism of action, antiviral drug promises and rule out against its treatment. *Journal of Biomolecular Structure & Dynamics*. <https://doi.org/10.1080/07391102.2020.1758788>
- Bzowka, M., Mitusińska, K., Raczynska, A., Samol, A., Tuszyński, J. A., & Gora, A. (2020). Structural and evolutionary analysis indicate that the SARS-CoV-2 Mpro is a challenging target for small-molecule inhibitors design. *International Journal of Molecular Sciences*, 21(9), 3099. <https://doi.org/10.3390/ijms21093099>
- Case, D. A., Belfon, K., Ben-Shalom, I. Y., Brozell, S. R., Cerutti, D. S., Cheatham, T. E., Cruzeiro, III, V. W. D., Darden, T. A., Duke, R.E., Giambasi, G., Gilson, M. K., Gohlke, H., Goetz, A. W., Harris, R, Izadi, S., Izmailov, S. A., Kasavajhala, K., Kovalenko, A., Krasny, R., ... Kollman, P. A. (2020). *AMBER 2020*. University of California.
- Chan, J. F.-W., Yuan, S., Kok, K.-H., To, K. K.-W., Chu, H., Yang, J., Xing, F., Liu, J., Yip, C. C.-Y., Poon, R. W.-S., Tsoi, H.-W., Lo, S. K.-F., Chan, K.-H., Poon, V. K.-M., Chan, W.-M., Ip, J. D., Cai, J.-P., Cheng, V. C.-C., Chen, H., Hui, C. K.-M., & Yuen, K.-Y. (2020). A familial cluster of pneumonia associated with the 2019 novel coronavirus indicating person-to-person transmission: A study of a family cluster. *Lancet (London, England)*, 395(10223), 514–523. [https://doi.org/10.1016/S0140-6736\(20\)30154-9](https://doi.org/10.1016/S0140-6736(20)30154-9)
- Chang, G. (2010). Quaternary structure of the SARS coronavirus main protease. In Lal, S. (Ed.), *Molecular Biology of the SARS-Coronavirus*, 115–128. Heidelberg, Berlin: Springer. https://doi.org/10.1007/978-3-642-03683-5_8
- Chen, Y., Liu, Q., & Guo, D. (2020). Emerging coronaviruses: Genome structure, replication, and pathogenesis. *Journal of Medical Virology*, 92(4), 418–423. <https://doi.org/10.1002/jmv.25681>
- De Wit, E., van Doremalen, N., Falzarano, D., & Munster, V. J. (2016). SARS and MERS: Recent insights into emerging coronaviruses. *Nature Reviews Microbiology*, 14(8), 523–534. <https://doi.org/10.1038/nrmicro.2016.81>
- Durrant, J. D., & McCammon, J. A. (2011). BINANA: A novel algorithm for ligand-binding characterization. *Journal of Molecular Graphics & Modelling*, 29(6), 888–893. <https://doi.org/10.1016/j.jmkgm.2011.01.004>
- Durrant, J. D., & McCammon, J. A. (2011). NNScore 2.0: A neural-network receptor-ligand scoring function. *Journal of Chemical Information and Modeling*, 51(11), 2897–2903. <https://doi.org/10.1021/ci2003889>
- Enmozhi, S. K., Raja, K., Sebastine, I., & Joseph, J. (2020). Andrographolide as a potential inhibitor of SARS-CoV-2 main protease: An in silico approach. *Journal of Biomolecular Structure & Dynamics*. <https://doi.org/10.1080/07391102.2020.1760136>
- Essmann, U., Perera, L., Berkowitz, M. L., Darden, T., Lee, H., & Pedersen, L. G. (1995). A smooth particle mesh Ewald method. *The Journal of Chemical Physics*, 103(19), 8577–8593. <https://doi.org/10.1063/1.470117>
- Fischer, A., Sellner, M., Naranjan, S., Lill, M. A., & Smiesko, M. (2020). Inhibitors for novel coronavirus protease identified by virtual screening of 687 million compounds. *ChemRxiv*. <https://doi.org/10.26434/chemrxiv.11923239.v1>
- Forster, P., Forster, L., Renfrew, C., & Forster, M. (2020). Phylogenetic network analysis of SARS-CoV-2 genomes. *Proceedings of the National Academy of Sciences*, 117(17), 9241–9243. <https://doi.org/10.1073/pnas.2004999117>
- Genheden, S., & Ryde, U. (2015). The MM/PBSA and MM/GBSA methods to estimate ligand-binding affinities. *Expert Opinion on Drug Discovery*, 10(5), 449–461. <https://doi.org/10.1517/17460441.2015.1032936>
- Golbraikh, A., Wang, X. S., Zhu, H., & Tropsha, A. (2017). Predictive QSAR modeling: Methods and applications in drug discovery and chemical risk assessment. In J. Leszczynski, A. Kaczmarek-Kedziera, T. Puzyn, G. M. Papadopoulos, H. Reis, K. M. Shukla (Eds.), *Handbook of computational chemistry*, 2303–2340. Springer.
- Gupta, M. K., Vemula, S., Donde, R., Gouda, G., Behera, L., & Vadde, R. (2020). *In-silico* approaches to detect inhibitors of the human severe acute respiratory syndrome coronavirus envelope protein ion channel. *Journal of Biomolecular Structure & Dynamics*. <http://doi.org/10.1080/07391102.2020.1751300>
- Hegyi, A., & Ziebuhr, J. (2002). Conservation of substrate specificities among coronavirus main proteases. *The Journal of General Virology*, 83(Pt 3), 595–599. <https://doi.org/10.1099/0022-1317-83-3-595>
- Hendaus, M. A. (2020). Remdesivir in the treatment of Coronavirus Disease 2019 (COVID-19): A simplified summary. *Journal of Biomolecular Structure & Dynamics*. <https://doi.org/10.1080/07391102.2020.1767691>
- Høyvik, I.-M., Jansik, B., & Jørgensen, P. (2012). Trust region minimization of orbital localization functions. *Journal of Chemical Theory and Computation*, 8(9), 3137–3146. <https://doi.org/10.1021/ct300473g>
- Islam, R., Parves, R., Paul, A. S., Uddin, N., Rahman, M. S., Mamun, A. A., Hossain, M. N., Ali, M. A., & Halim, M. A. (2020). A molecular modeling approach to identify effective antiviral phytochemicals against the main protease of SARS-CoV-2. *Journal of Biomolecular Structure & Dynamics*. <https://doi.org/10.1080/07391102.2020.1761883>
- Jin, Z., Du, X., Xu, Y., Deng, Y., Liu, M., Zhao, Y., Zhang, B., Li, X., Zhang, L., Peng, C., Duan, Y., Yu, J., Wang, L., Yang, K., Liu, F., Jiang, R., Yang, X., You, T., Liu, X., ... Yang, H. (2020). Structure of M^{Pro} from 1 COVID-19 virus and discovery of its inhibitors. *Nature*, 582(7811), 289–293. <https://doi.org/10.1038/s41586-020-2223-y>
- Jorgensen, W. L., Chandrasekhar, J., Madura, J. D., Impey, R. W., & Klein, M. L. (1983). Comparison of simple potential functions for simulating liquid water. *The Journal of Chemical Physics*, 79(2), 926–935. <https://doi.org/10.1063/1.445869>
- Joshi, R. S., Jagdale, S. S., Bansode, S. B., Shankar, S. S., Tellis, M. B., Pandya, V. P., Chugh, A., Giri, A. P., & Kulkarni, M. J. (2020). Discovery of potential multi-target-directed ligands by targeting host-specific SARS-CoV-2 structurally conserved main protease. *Journal of Biomolecular Structure & Dynamics*. <https://doi.org/10.1080/07391102.2020.1760137>
- Khailany, R. A., Safdar, M., & Ozaslan, M. (2020). Genomic characterization of a novel SARS-CoV-2. *Gene Reports*, 19, 100682. <https://doi.org/10.1016/j.genrep.2020.100682>
- Khan, S. A., Zia, K., Ashraf, S., Uddin, R., & Ul-Haq, Z. (2020). ^a. Identification of chymotrypsin-like protease inhibitors of SARS-CoV-2 via integrated computational approach. *Journal of Biomolecular Structure & Dynamics*. <https://doi.org/10.1080/07391102.2020.1751298>
- Khan, R. J., Jha, R. K., Amera, G. M., Jain, M., Singh, E., Pathak, A., Singh, R. P., Muthukumar, J., & Singh, A. K. (2020). Targeting SARS-CoV-2: A systematic drug repurposing approach to identify promising inhibitors against 3C-like proteinase and 2'-O-ribose methyltransferase. *Journal of Biomolecular Structure & Dynamics*. <https://doi.org/10.1080/07391102.2020.1753577>
- Klamt, A. (2005). *COSMO-RS: From quantum chemistry to fluid phase thermodynamics and drug design* (1st ed., p. 246). Elsevier.
- Klamt, A., Moya, C., & Palomar, J. (2015). A comprehensive comparison of the IEFPCM and SS(V)PE continuum solvation methods with the COSMO approach. *Journal of Chemical Theory and Computation*, 11(9), 4220–4225. <https://doi.org/10.1021/acs.jctc.5b00601>
- Klamt, A., & Schüürmann, G. (1993). COSMO: A new approach to dielectric screening in solvents with explicit expressions for the screening energy and its gradient. *Journal of the Chemical Society, Perkin Transactions*, 2, 799–805.
- Kuseva, C., Schultz, T. W., Yordanova, D., Tankova, K., Kutsarova, S., Pavlov, T., Chapkanov, A., Georgiev, M., Gissi, A., Sobanski, T., & Mekenyan, O. G. (2019). The implementation of RAAF in the OECD

- QSAR Toolbox. *Regular Toxicology & Pharmacology*, 105, 51–61. <https://doi.org/10.1016/j.yrtph.2019.03.018>
- Lehtola, S., & Jónsson, H. (2013). Unitary optimization of localized molecular orbitals. *Journal of Chemical Theory and Computation*, 9(12), 5365–5372. <https://doi.org/10.1021/ct400793q>
- Lipinski, C. A., Lombardo, F., Dominy, B. W., & Feeney, P. J. (2001). Experimental and computational approaches to estimate solubility and permeability in drug discovery and development settings. *Advanced Drug Delivery Reviews*, 46(1–3), 3–26. PMID: 11259830 [https://doi.org/10.1016/s0169-409x\(00\)00129-0](https://doi.org/10.1016/s0169-409x(00)00129-0)
- Liu, X., & Wang, X.-J. (2020). Potential inhibitors for 2019-nCoV coronavirus M protease from clinically approved medicines. *BioRxiv*. <https://doi.org/10.1101/2020.01.29.924100>
- Lu, R., Zhao, X., Li, J., Niu, P., Yang, B., Wu, H., Wang, W., Song, H., Huang, B., Zhu, N., Bi, Y., Ma, X., Zhan, F., Wang, L., Hu, T., Zhou, H., Hu, Z., Zhou, W., Zhao, L., ... Tan, W. (2020). Genomic characterisation and epidemiology of 2019 novel coronavirus: Implications for virus origins and receptor binding. *Lancet (London, England)*, 395(10224), 565–574. [https://doi.org/10.1016/S0140-6736\(20\)30251-8](https://doi.org/10.1016/S0140-6736(20)30251-8)
- McDonald, I. K., & Thornton, J. M. (1994). Satisfying hydrogen bonding potential in proteins. *Journal of Molecular Biology*, 238(5), 777–793. <https://doi.org/10.1006/jmbi.1994.1334>
- Muralidharan, N., Sakthivel, R., Velmurugan, D., & Gromiha, M. M. (2020). Computational studies of drug repurposing and synergism of lopinavir, oseltamivir and ritonavir binding with SARS-CoV-2 Protease against COVID-19. *Journal of Biomolecular Structure & Dynamics*. <https://doi.org/10.1080/07391102.2020.1752802>
- Olubiyi, O. O., Olagunju, M., Keutmann, M., Loschwitz, J., & Strodel, B. (2020). High throughput virtual screening to discover inhibitors of the main protease of the coronavirus SARS-CoV-2. *Preprint from Preprints.org*. <https://doi.org/10.20944/preprints202004.0161.v1>
- Pachetti, M., Marini, B., Benedetti, F., Giudici, F., Mauro, E., Storici, P., Masciovecchio, C., Angeletti, S., Ciccocozzi, M., Gallo, R. C., Zella, D., & Ippodrino, R. (2020). Emerging SARS-CoV-2 mutation hot spots include a novel RNA-dependent-RNA polymerase variant. *Journal of Translational Medicine*, 18(1), 179. <https://doi.org/10.1186/s12967-020-02344-6>
- Pant, S., Singh, M., Ravichandiran, V., Murty, U. S. N., & Srivastava, H. K. (2020). Peptide-like and small-molecule inhibitors against Covid-19. *Journal of Biomolecular Structure & Dynamics*. <https://doi.org/doi:10.1080/07391102.2020.1757510>
- Pettersen, E. F., Goddard, T. D., Huang, C. C., Couch, G. S., Greenblatt, D. M., Meng, E. C., & Ferrin, T. E. (2004). UCSF Chimera—a visualization system for exploratory research and analysis. *Journal of Computational Chemistry*, 25(13), 1605–1612. <https://doi.org/10.1002/jcc.20084>
- Pillaiyar, T., Manickam, M., Namasivayam, V., Hayashi, Y., & Jung, S. H. (2016). An overview of Severe Acute Respiratory Syndrome-Coronavirus (SARS-CoV) 3CL protease inhibitors: Peptidomimetics and small molecule chemotherapy. *Journal of Medicinal Chemistry*, 59(14), 6595–6628. <https://doi.org/10.1021/acs.jmedchem.5b01461>
- Qamar, M. T., Alqahtani, S. M., Alamri, M. A., & Chen, L.-L. (2020). Structural basis of SARS-CoV-2 3CL^{pro} and anti-COVID-19 drug discovery from medicinal plants. *Journal of Pharmaceutical Analysis*. <https://doi.org/10.1016/j.jpha.2020.03.009>
- Rappe, A. K., Casewit, C. J., Colwell, K. S., Goddard, W. A., III, & Skiff, W. M. (1992). UFF, a full periodic table force field for molecular mechanics and molecular dynamics simulations. *Journal of the American Chemical Society*, 114(25), 10024–10035. <https://doi.org/10.1021/ja00051a040>
- Rismanbaf, A. (2020). Potential treatments for COVID-19; a narrative literature review. *Archives of Academic Emergency Medicine*, 8(1), e29.
- Ryckaert, J. P., Ciccotti, G., & Berendsen, H. J. C. (1977). Numerical integration of the Cartesian equations of motion of a system with constraints: Molecular dynamics of n-alkanes. *Journal of Computational Physics*, 23(3), 327–341. [https://doi.org/10.1016/0021-9991\(77\)90098-5](https://doi.org/10.1016/0021-9991(77)90098-5)
- Sarma, P., Sekhar, N., Prajapat, M., Avti, P., Kaur, H., Kumar, S., Singh, S., Kumar, H., Prakash, A., Dhibar, D. P., & Medhi, B. (2020). In-silico homology assisted identification of inhibitor of RNA binding against 2019-nCoV N-protein (N terminal domain). *Journal of Biomolecular Structure & Dynamics*. <https://doi.org/10.1080/07391102.2020.1753580>
- Schultz, T. W., Diderich, R., Kuseva, C. D., & Mekenyan, O. G. (2018). The OECD QSAR Toolbox starts its second decade. *Methods in Molecular Biology (Clifton, N.J.)*, 1800, 55–77. https://doi.org/10.1007/978-1-4939-7899-1_2
- Sharma, G., & First, E. A. (2009). Thermodynamic analysis reveals a temperature-dependent change in the catalytic mechanism of bacillus stearothermophilus tyrosyl-tRNA synthetase. *The Journal of Biological Chemistry*, 284(7), 4179–4190. <https://doi.org/10.1074/jbc.M808500200>
- Stewart, J. J. P. (2013). Optimization of parameters for semiempirical methods VI: More modifications to the NDDO approximations and re-optimization of parameters. *Journal of Molecular Modeling*, 19(1), 1–32. <https://doi.org/10.1007/s00894-012-1667-x>
- Sun, H., Li, Y., Tian, S., Xu, L., & Hou, T. (2014). Assessing the performance of MM/PBSA and MM/GBSA methods. 4. Accuracies of MM/PBSA and MM/GBSA methodologies evaluated by various simulation protocols using PDBbind data set. *Physical Chemistry Chemical Physics : Pccp*, 16(31), 16719–16729. <https://doi.org/10.1039/c4cp01388c>
- Sunseri, J., & Koes, D. R. (2016). Pharmit: Interactive exploration of chemical space. *Nucleic Acids Research*, 44(W1), W442–W448. <https://doi.org/10.1093/nar/gkw287>
- Ton, A.-T., Gentile, F., Hsing, M., Ban, F., & Cherkasov, A. (2020). Rapid identification of potential inhibitors of SARS-CoV-2 main protease by deep docking of 1.3 billion compounds. *Molecular Informatics*. <https://doi.org/10.1002/minf.202000028>
- Vega-Valdez, I. R., Santiago-Quintana, J. M., Rosalez, M. N., Farfan-Garcia, E. D., & Soriano-Ursua, M. A. (2020). Theoretical evaluation of bortezomib and other boron-containing compounds as inhibitors of SARS-CoV-2 main protease. *ChemRxiv*. <https://doi.org/10.26434/chemrxiv.12047346.v1>
- Wahedi, H. M., Ahmad, S., & Abbasi, S. W. (2020). Stilbene-based natural compounds as promising drug candidates against COVID-19. *Journal of Biomolecular Structure & Dynamics*. <https://doi.org/10.1080/07391102.2020.1762743>
- Wang, J., Wolf, R. M., Caldwell, J. W., Kollman, P. A., & Case, D. A. (2004). Development and testing of a general Amber force field. *Journal of Computational Chemistry*, 25(9), 1157–1174. <https://doi.org/10.1002/jcc.20035>
- Xu, L., Sun, H., Li, Y., Wang, J., & Hou, T. (2013). Assessing the performance of MM/PBSA and MM/GBSA methods. 3. The impact of force fields and ligand charge models. *The Journal of Physical Chemistry. B*, 117(28), 8408–8421. <https://doi.org/10.1021/jp404160y>
- Yan, L., Zhang, J., Wang, N., Li, H., Shi, Y., Guo, ... Zou, Q. (2020). Therapeutic drugs targeting 2019-nCoV main protease by high-throughput screening. *BioRxiv*. <https://doi.org/10.1101/2020.01.28.922922>
- Yang, H., Yang, M., Ding, Y., Liu, Y., Lou, Z., Zhou, Z., Sun, L., Mo, L., Ye, S., Pang, H., Gao, G. F., Anand, K., Bartlam, M., Hilgenfeld, R., & Rao, Z. (2003). The crystal structures of severe acute respiratory syndrome virus main protease and its complex with an inhibitor. *Proceedings of the National Academy of Sciences of the United States of America*, 100(23), 13190–13195. <https://doi.org/10.1073/pnas.1835675100>
- Yao, H., Lu, X., Chen, O., Xu, K., Chen, Y., Cheng, L., & Li, L. (2020). Patient-derived mutations impact pathogenicity of SARS-CoV-2. *MedRxiv*. <https://doi.org/10.1101/2020.04.14.20060160>
- Zhang, L., Lin, D., Sun, X., Curth, U., Drosten, C., Sauerhering, L., Becker, S., Rox, K., & Hilgenfeld, R. (2020). Crystal structure of SARS-CoV-2 main protease provides a basis for design of improved α -ketoamide inhibitors. *Science (New York, N.Y.)*, 368(6489), 409–412. <https://doi.org/10.1126/science.abb3405>
- Zhijian, X., Peng, C., Shi, Y., Zhu, Z., Mu, K., Wang, X., & Zhu, W. (2020). Nelfinavir was predicted to be a potential inhibitor of 2019-nCoV main protease by an integrative approach combining homology modelling, molecular docking and binding free energy calculation. *BioRxiv*. <https://doi.org/10.1101/2020.01.27.921627>
- Zhou, Y., Hou, Y., Shen, J., Huang, Y., Martin, W., & Cheng, F. (2020). Network-based drug repurposing for novel coronavirus 2019-nCoV/SARS-CoV-2. *Cell Discovery*, 6(1), 14. <https://doi.org/10.1038/s41421-020-0153-3>